Journal of Metastable and Nanocrystalline Materials
ISSN: 2297-6620, Vols. 15-16, pp 93-98
doi:10.4028/www.scientific.net/JMNM.15-16.93

Online: 2003-04-10

Magnetic Properties and Magnetic Domain Structure of Nd-Fe Based Metallic Glasses

B.C. Wei[1*], G.S. Yu[2], L. Xia[3], M.X. Pan[3], B.S. Han[3] and W.H. Wang[3]

[1] National Microgravity Laboratory, Institute of Mechanics, Chinese Academy of Sciences, Beijing 100080, China P.R.

[2] Faculty of Materials and Photoelectronic Physics, Xiangtan University, Xiangtan 411105, China P.R.

[3] Institute of Physics and Center for Condensed Matter Physics, Chinese Academy of Sciences, Beijing 100080, China P.R.

Keywords: Bulk Metallic Glasses, Hard Magnetic Properties, Magnetic Domains, Magnetic Force Microscopy

Abstract. The transition from hard to soft magnetic behavior with increasing quenching rate is shown for $Nd_{60}Al_{10}Fe_{20}Co_{10}$ rods and melt-spun ribbons with different thickness. Microstructures characterized by high resolution transmission electron microscopy (HRTEM) show that clusters with a size from 1 to 5 nm randomly distribute in the amorphous matrix in the samples prepared by different quenching rate. By compared the magnetic behaviors with those of fully crystalline $Nd_{70}Fe_{30}$ alloy, it is found that the clusters with a local ordering similar to the A1 metastable Nd-Fe binary phase is responsible for the hard magnetic properties in samples subjected to relatively low quenching rate. Magnetic domain structure of $Nd_{60}Al_{10}Fe_{20}Co_{10}$ and $Nd_{70}Fe_{30}$ alloys were studied by high resolution magnetic force microscopy (MFM). The magnetic hardening mechanism of $Nd_{60}Al_{10}Fe_{20}Co_{10}$ bulk metallic glasses is discussed.

1. Introduction

A number of new metallic alloys with excellent glass forming ability have been developed in the last ten years, and it permits the formation of large bulky ingots of metallic glass [1-3]. More recently, Nd(Pr)-Fe-Al family bulk metallic glasses (BMGs) of a diameter up to 12 mm with interesting magnetic properties have been reported. High coercivity values have been measured in bulk amorphous rods formed under a relatively low quenching rate, while the melt-spun ribbons with same composition prepared at a high quenching rate exhibit soft magnetic properties [4-15]. The hard magnetic properties of the amorphous Nd(Pr)-Fe-Al based alloys are interesting in both scientific and practical viewpoints. However, the mechanisms responsible for the hard magnetic properties of the Nd(Pr)-based BMGs and the relationship between microstructure and magnetic properties are still not clear. In this study, $Nd_{60}Al_{10}Fe_{20}Co_{10}$ rods with 5 mm in diameter and melt-spun ribbons with different quenching rates were prepared. The effect of quenching rate on the magnetic properties of $Nd_{60}Al_{10}Fe_{20}Co_{10}$ amorphous alloys was systematically investigated. A magnetic force microscopy (MFM) was used to study the magnetic domain structures of these novel metallic glasses. In order to reveal the magnetic hardening mechanism of the present Nd-Fe-Al-Co metallic glass, magnetic properties of a crystalline Nd-Fe binary eutectic alloy were also studied for comparison.

2. Experiments

Ingots of $Nd_{60}Al_{10}Fe_{20}Co_{10}$ and $Nd_{70}Fe_{30}$ alloys were prepared by arc-melting a mixture of the pure elements Nd, Al, Fe and Co with a purity of at least 99.9% in titanium-gettered argon atmosphere. Cylindrical specimens of 5 mm in diameter and 70 mm in length were prepared from the pre-alloyed ingots by suction casting into a copper mold. Ribbons were obtained by melt-spinning using a single copper wheel under pure argon atmosphere. The surface speed of the

*Corresponding author: weibc@imech.ac.cn (B. C. Wei)

copper wheel was varied from 3 to 42 m/s, and the corresponding thickness of the ribbon varies from 200 to 28 μm. The structure of the samples was characterized by X-ray diffraction (XRD) using Cu K_α radiation. A closer investigation of microstructure was undertaken with high resolution transmission electron microscopy (HRTEM). Thermal analysis was performed with a Perkin-Elmer DSC 7 differential scanning calorimeter under argon atmosphere. The magnetic polarization as a function of the magnetic field was measured at room temperature using a vibrating sample magnetometer (VSM) with maximum applied field of 1592 kAm^{-1}. The Curie temperatures were measured with a Faraday magnetometer at a heating rate of 0.17 K/s. The study of the domain structure was carried out by using a Digital Instruments NanoScope IIIa D-3000 magnetic force microscope (MFM). It allows the topographic and magnetic force images to be collected separately and simultaneously in the same area of the sample by using Tapping/Lift modes. The magnetic tips used were micro-fabricated Si cantilevers with a pyramidal tip coated with magnetic Co-Cr thin film of 40 nm thickness and a coercivity of about 32 kAm^{-1}. In our experiments, the tip used was magnetized downward prior to imaging. Its lift-height during scanning was 30 nm. Further details regarding the MFM experiments are given in Ref. 9. The ribbons were studied on their non-contact side without any pre-treatment.

3. Results and discussion

Fig. 1 shows the hysteresis loops of $Nd_{60}Al_{10}Fe_{20}Co_{10}$ rod and ribbons melt-spun at different wheel speed. The inset exhibits the XRD patterns of the as-cast rod and ribbon melt spun at 30 m/s. It is revealed that all the samples prepared at different quenching rate comprise a large fraction of amorphous phase. The profile of hysteresis loops of $Nd_{60}Al_{10}Fe_{20}Co_{10}$ alloy changes with increasing quenching rate. The as-cast BMG exhibits coercivity (H_c) of 326 kAm^{-1}, saturation magnetization under external field of 1592 kAm^{-1} (J_s) of 1.61 T and remanent magnetization (J_r) of 0.107 T. For the ribbons, H_c decreases gradually from 180 kA/m to 18.5 kA/m with the wheel speed increasing from 3 m/s to 30 m/s. J_s and J_r slope down continuously with rising quenching rate, from 0.156 T and 0.087 T for the 3 m/s ribbon to 0.080 T and 0.018 T for the 30 m/s ribbon, respectively.

The representative micrograph of the 5 mm as-cast rod measured by HRTEM is shown in Fig. 2. A large number of ordered clusters with an average size of about 5 nm are observed to randomly

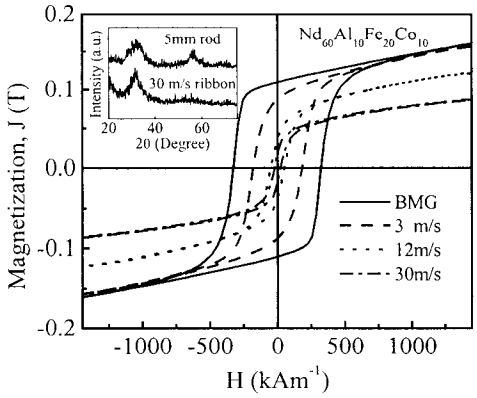

Fig 1. Hysteresis loops at room temperature of $Nd_{60}Al_{10}Fe_{20}Co_{10}$ BMG and ribbons melt spun at different wheel speed. The inset shows the XRD patterns of the 5 mm rod and the ribbon at 30 m/s

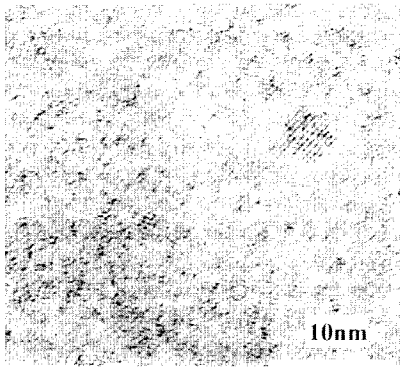

Fig. 2. HRTEM image of 5 mm $Nd_{60}Al_{10}Fe_{20}Co_{10}$ BMG rod

distribute in the amorphous matrix. These ordered structures are quite small, and are not reflected within the detection limit of XRD measurements. The size of the clusters decreases continuously with increasing quenching rate, and is 1~2 nm in the ribbon sample melt-spun at 18 m/s. This means that there are at least two phases, i.e. disorder amorphous phase and ordered clusters, existed in the alloys prepared by different route.

In order to clarify that which phase, amorphous phase or ordered clusters, is responsible for the hard magnetic properties of the alloy. The magnetic properties of the $Nd_{70}Fe_{30}$ alloy with relatively weak glass forming ability are studied, and the results are shown in Fig. 3. The binary alloy also exhibits hard magnetic properties at room temperature with H_c of 335, 239 and 102 kAm^{-1} for ribbons melt-spun at 12, 18 and 30 m/s, respectively. Though H_c, J_s and J_r of the binary alloy are higher than those of the $Nd_{60}Al_{10}Fe_{20}Co_{10}$ alloy, the same tendency of hard magnetic properties decreasing with the increase of quenching speed is observed. The XRD patterns of the binary alloy ribbons are shown in the inset of Fig. 3. Typical crystalline features are observed for the three alloys. DSC results prove that no crystallization processes is observed below 873 K for the three samples. These indicate that there is no amorphous phase existed in the three samples. In other words, crystalline phases are responsible for the hard magnetic properties of the present binary alloy. In fact, Owing to the important role of the binary Nd-Fe eutectic in governing the magnetic properties of Nd-Fe-B permanent magnets, the mechanism responsible for the hard properties and microstructure of Nd-rich Nd-Fe binary alloys have already been studied in detail. Most of these results support that the high coercivity can be attributed to the presence of a metastable highly anisotropic iron-rich A1 phase [16-19]. This phase was not identified in XRD spectra, but its presence has been confirmed by thermomagnetic analysis (TMA). The Curie temperature (T_c) of the A1 phase is near 513 K [17-19]. The Curie temperatures of the present binary samples are shown in the lower inset of Fig. 3. The T_c values of the three alloys, especially the ribbon melt-spun at lower speed, agree well with that of A1 phase. This confirms that the high H_c of the present binary alloy can be attributed to the presence of a high anisotropic A1 phase. The difference in coercivity measured at room temperature (Fig. 3) may be related to different compositions obtained as the quenching rate varies, as spin coupling and the magnetic anisotropy are expected to be strongly dependent on the composition. This is proved by the dependence of T_c on the melt-spinning rate, that is, T_c significantly decreases with increasing quenching rate, indicating the decreasing of iron content in Al phase.

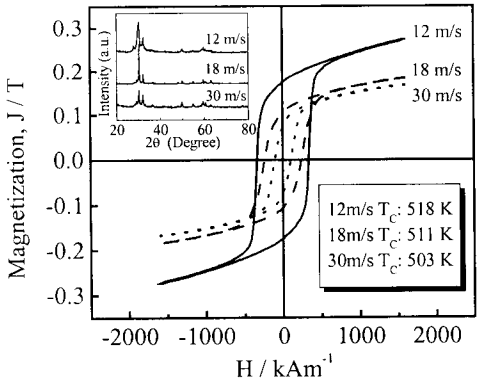

Fig. 3. Hysteresis loops of $Nd_{70}Fe_{30}$ ribbons melt spun at different wheel speeds. The insets show their XRD patterns and T_c values, respectively

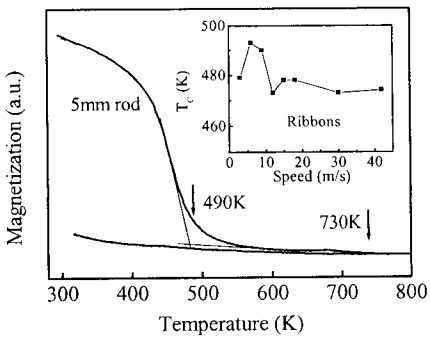

Fig. 4. Thermomagnetic analysis of 5 mm $Nd_{60}Al_{10}Fe_{20}Co_{10}$ BMG. Inset: T_c *vs* wheel rotating speed for ribbons.

The T_c values of the $Nd_{60}Al_{10}Fe_{20}Co_{10}$ samples prepared by different quenching rate differ from 473 to 494 K as shown in Fig. 4. These values are lower than that of A1 phase. The addition of aluminium to the Nd-Fe binary eutectic greatly enhances the glass forming ability (GFA), and the addition of cobalt into the Nd-Fe-Al system further improves the GFA [4,7]. This would suppress the crystallization of Al phase during cooling. Instead, cluster structures form as shown in Fig. 2. Consequently, we suggest that the presence of clusters, which has a similar local structure and composition as the A1 phase in Nd-Fe binary alloys, is responsible for the hard magnetic properties in samples subjected to relatively low quenching rates.

It is noted that the T_c of the $Nd_{60}Al_{10}Fe_{20}Co_{10}$ rod and ribbons melt-spun at different speeds does not show a distinct tendency of decreasing with increasing quenching rate (Fig. 4), though the strong tendency of coercivity to decrease with increasing quenching rate is indeed observed (Fig. 1). As T_c is sensitive to local chemical composition, there is no significant difference in the composition of clusters in samples prepared by different quenching rate. Thereby, the decrease of hard magnetic properties with increasing quenching rate can be only explained by the decrease of instinct anisotropy of clusters resulting from the compositional difference.

A study of the magnetic domain structure is useful for understanding micromagnetic mechanisms. Here, a MFM was employed to image the magnetic domain structure in as-cast rod and ribbons with different quenching rates. In Fig. 5a a typical 10×10 μm topographic (left) and magnetic force (right) images of the 5 mm $Nd_{60}Al_{10}Fe_{20}Co_{10}$ rod are presented. The magnetic force image is characterized by darker areas adjacent with brighter areas of sub-micron scale and a random distribution. The dark area indicates that the magnetization direction in this area is nearly

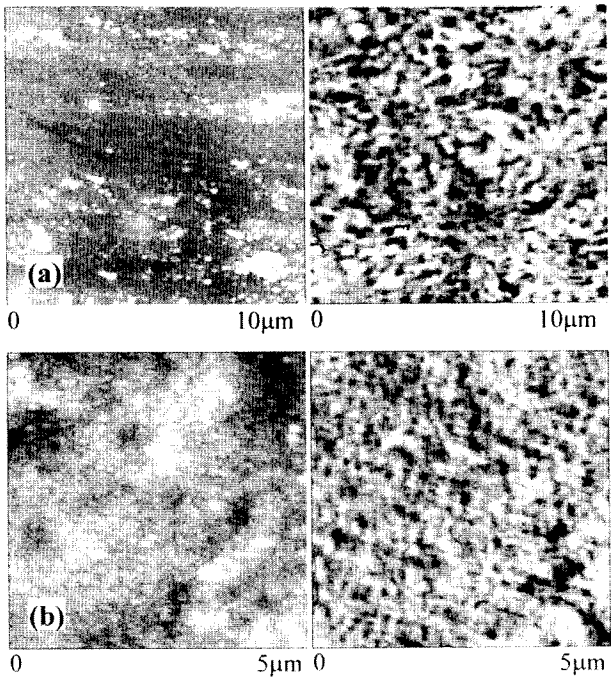

Fig. 5. The topography (left) and Magnetic force image (right) of 5 mm $Nd_{60}Al_{10}Fe_{20}Co_{10}$ BMG with a scan size 10 μm × 10μm (a), and $Nd_{70}Fe_{30}$ ribbon melt spun at 12 m/s with a scan size 5 μm × 5 μm (b)

parallel to the upward tip magnetization, and the bright area indicates the opposite. Several images taken from different positions of the sample surface show the similar domain feature. The average period (T) of the domain pattern and the average contrast between dark and bright areas were measured by means of section analysis, revealing $T \approx 530$ nm. The average roughness $(Ra)_{\Delta\phi}$ and the root mean square $(RMS)_{\Delta\phi}$ describing the contrast of the image are 1.39° and 1.18°, respectively.

It is important to note that the period of magnetic domain is considerable lager than that of the size of cluster in alloys. This indicates that the large areas of magnetic contrast are actually a collection of a group of clusters with similar magnetic orientation. The isolated clusters are correlated by some kind of interaction with each other. These are typical features of interaction type magnetic domain [20]. The $Nd_{60}Al_{10}Fe_{20}Co_{10}$ ribbons melt-spun at different speed show a similar magnetic domain period as the BMG, but the magnetic contrast decrease continuously with increasing quenching rate. A typical 5 × 5 μm MFM images of $Nd_{70}Fe_{30}$ melt spun at 12 m/s is shown in Fig. 5b. A much smaller domain period less than 300 nm is observed. The quite smaller magnetic contrast correlation length suggests that the interaction of clusters is reduced in the binary alloy. The mechanism for the interactions and how it affects the magnetic properties of Nd-Fe system alloys need further study. From the thermomagnetic curves of the $Nd_{60}Al_{10}Fe_{20}Co_{10}$ alloys (Fig. 4), one can see that above T_c the magnetization does not decrease to zero until about 730 K. This phenomenon can also be observed in results of Inoue et al. [4], indicating that a second magnetic phase may exist in the alloy. Hence, competing magnetic interactions may account for the complex magnetic properties of the alloy.

4. Summary

The magnetic properties of $Nd_{60}Al_{10}Fe_{20}Co_{10}$ amorphous like alloys are sensitive to the quenching rate. High coercivity is revealed for the bulk sample and thick ribbons, whereas thin ribbons are magnetically soft. The HRTEM images show clusters with a size of a few nanometers in the as-cast rod and melt-spun ribbons. The crystalline $Nd_{70}Fe_{30}$ binary alloy also exhibits hard magnetic properties at room temperature, and shows the similar dependence of coercivity on quenching rate. Clusters possessing a local chemical order similar to the metastable A1 phase known from the Nd-Fe binary system are supposed to be responsible for the hard magnetic properties in $Nd_{60}Al_{10}Fe_{20}Co_{10}$ prepared at lower quenching rates. Interaction type magnetic domain with a periodicity of about 530 nm is observed in $Nd_{60}Al_{10}Fe_{20}Co_{10}$ rods and ribbons irrespective the quenching rate.

Acknowledgments

The authors are grateful to W. Löser, S. Roth and J. Eckert for stimulating discussions. The financial supports of the National Nature Science Foundation of China (Grant Nos. 50101012 and 50031010) are appreciated.

References

[1] A. Inoue, T. Zhang and T. Masumoto, Mater. Trans., JIM, Vol. 31 (1990), p. 425.
[2] A. Inoue, T. Zhang, N. Nishiyama, K. Ohba and T. Masumoto, Mater. Trans. JIM, Vol. 33 (1992), p. 937.
[3] A. Peker and W. L. Johnson, Appl. Phys. Lett., Vol. 63 (1993), p. 2342.
[4] A. Inoue, T. Zhang, A. Takeuchi, and W. Zhang, Mater. Trans. JIM, Vol. 37 (1996), p. 636.
[5] A. Inoue, A. Takeuchi, and T. Zhang, Metall. and Mater. Trans. Vol. 29A (1998), p. 1779.
[6] Y. Li, S. C. Ng, Z. P. Lu, Y. P. Feng, and K. Lu, Phil. Mag. Lett. Vol. 78 (1998), p. 213.
[7] L. Q. Xing, J. Eckert, W. Löser, S. Roth, and L. Schultz, J. Appl. Phys. Vol. 88 (2000), p. 3565.
[8] H. Chiriac, N. Lupu, J. Non-Cryst. Solids, Vol. 287 (2001), p. 135.
[9] B. C. Wei, W. H. Wang, M. X. Pan, B. S. Han, Z. R. Zhang, and W. R. Hu, Phys. Rev. B, Vol.

64 (2001), 012406.
[10] B. C. Wei, Y. Zhang, Y. X. Zhuang, D. Q. Zhao, M. X. Pan, W. H. Wang, and W. R. Hu, J. Appl. Phys. Vol. 89 (2001), p. 3529.
[11] B. C. Wei, W. H. Wang, L. Xia, Z. Zhang, D. Q. Zhao, and M. X. Pan, Mater. Sci. Eng. Vol. A334 (2002), p. 307
[12] B. C. Wei, W. Löser, L. Xia, S. Roth, M. X. Pan, W. H. Wang and J. Eckert, Acta mater. Vol. 50 (2002), p. 4357
[13] G. Kumar, J. Eckert, S. Roth, W. Löser, S. Ram, L. Schultz, J. Appl. Phys. Vol. 91 (2002), p. 3764
[14] Z. G. Sun, W. Löser, J. Eckert, K,-H. Müller, L. Schultz, Appl. Phys. Lett. Vol. 80 (2002), p. 772
[15] R. J. Ortega-Hertogs, A. Inoue, and K. V. Rao, Scripta mater. Vol. 44 (2001), p. 1333.
[16] J. J. Croat, J. Appl. Phys. Vol. 52 (1981), p. 2509.
[17] J. L. S. Llamazares, F. Leccabue, F. Bolzoni, R. Panizzieri, and X. R. Hua, J. Magn. Magn. Mater. Vol. 84 (1990), p. 79
[18] J. Delamare, D. Lemarchand, and P. Vigier, J. Alloy Comp. Vol. 216 (1994), p. 273.
[19] V. P. Menushenkov, S. J. Andersen, and R. Høier, Proceedings of the 10th International Symposium on Magnetic Anisotropy and Coercivity in Rare-Earth Transition Metal Alloys, Dresden, Werkstoff-Informationsgesellschaft, (1998), p. 97.
[20] M .A. Al-Khafaji, W. M. Rainforth, M. R. J. Gibbs, H. A. Davies and J. E. L. Bishop, J. Magn. Magn. Mater. Vol. 182 (1998), p. 111.

Metastable, Mechanically Alloyed and Nanocrystalline Materials 2002
10.4028/www.scientific.net/JMNM.15-16

Magnetic Properties and Magnetic Domain Structure of Nd-Fe Based Metallic Glasses
10.4028/www.scientific.net/JMNM.15-16.93